Biol. Chem., Vol. 381, pp. 993–999, September/October 2000

Helical Tubes of FtsZ from *Methanococcus jannaschii*

Jan Löwe* and Linda A. Amos

MRC Laboratory of Molecular Biology, Hills Road, Cambridge CB2 2QH, UK

* Corresponding author

Bacterial cell division depends on the formation of a cytokinetic ring structure, the Z-ring. The bacterial tubulin homologue FtsZ is required for Z-ring formation. FtsZ assembles into various polymeric forms *in vitro,* indicating a structural role in the septum of bacteria. We have used recombinant FtsZ1 protein from *M. jannaschii* to produce helical tubes and sheets with high yield using the GTP analogue GMPCPP [guanylyl-(α,β)-methylene-diphosphate]. The sheets appear identical to the previously reported Ca^{++}-induced sheets of FtsZ from *M. jannaschii* that were shown to consist of 'thick'-filaments in which two protofilaments run in parallel. Tubes assembled either in Ca^{++} or in GMPCPP contain filaments whose dimensions indicate that they could be equivalent to the 'thick'-filaments in sheets. Some tubes are hollow but others are filled by additional protein density. Helical FtsZ tubes differ from eukaryotic microtubules in that the filaments curve around the filament axis with a pitch of ~ 430 Å for Ca^{++}-induced tubes or 590 – 620 Å for GMPCPP. However, their assembly *in vitro* as well-ordered polymers over distances comparable to the inner circumference of a bacterium may indicate a role *in vivo*. Their size and stability make them suitable for use in motility assays.

Key words: Helical reconstruction / Microtubules / Tubulin.

Introduction

For a bacterium to divide the cell envelope must be moved inwards to yield two daughter cells, a process called septation (review: Donachie, 1993). For septation to proceed, a number of proteins assemble at the site of septum formation in a specific sequence (recent reviews: Bramhill, 1997; Lutkenhaus and Addinall, 1997; Rothfield *et al*., 1999). After the site for the septum has been selected using the MinCDE system, FtsZ is the first protein known to appear at the septum. FtsZ then directs all other known septum proteins including ZipA, FtsA, FtsQ, FtsW, FtsI, FtsL, FtsK, and possibly others. FtsZ assembles into a ring structure *in vivo* as seen by light microscopy of cells and assembles into filaments *in vitro*, indicating a structural role for FtsZ in cell division. Further evidence for a structural role comes from the fact that FtsZ can be regarded as the bacterial homologue of the eukaryotic cytoskeletal protein tubulin (Erickson, 1995). Tubulin and FtsZ share a common three-dimensional structure (Löwe and Amos, 1998; Nogales *et al*., 1998b) and form protofilaments in which the longitudinal contact enhances GTP hydrolysis, thus providing a mechanism for polymerisation dependent GTPase regulation (Erickson, 1998; Nogales *et al*., 1998a). A 6-residue insertion in the β-strand preceding loop T2 in FtsZ (Nogales *et al*., 1998a) produces a phenotype that shows FtsZ spirals instead of closed rings inside cells, indicating that FtsZ acts as a structural protein directly guiding the formation of the septum (Bi and Lutkenhaus, 1992; Addinall and Lutkenhaus, 1996). The homology to tubulin initiated a search for motor proteins in prokaryotes that move on FtsZ tracks. No obvious candidate has been found so far. A major problem in the field arises from the fact that no ultrastructural information about the *in vivo* structure of the FtsZ polymer is available. This is due to the small size of the septum and the high protein density near the septum. In the meantime, *in vitro* experiments have found a number of FtsZ polymers (Bramhill and Thompson, 1994; Mukherjee and Lutkenhaus, 1994; Erickson, 1995; Erickson *et al*., 1996; Yu and Margolin, 1997; Lu *et al*., 1998; Mukherjee and Lutkenhaus, 1998; Trusca *et al*., 1998; Löwe and Amos, 1999) that may be related to the *in vivo* polymer, although it should be kept in mind that *in vivo* FtsZ polymerisation may be guided by additional factors. Single, curved filaments have been obtained by polymerising FtsZ in solution in the presence of GTP (Lu *et al*., 1998, 2000; Mukherjee and Lutkenhaus, 1998). When performed on a lipid monolayer, FtsZ polymerisation yielded minirings (Erickson *et al*., 1996). Sheets of laterally aligned filaments have been obtained under many conditions: in the presence of Ca^{++} (Yu and Margolin, 1997; Löwe and Amos, 1999), DEAE dextran (Erickson *et al*., 1996), and GTP alone. A low resolution three-dimensional reconstruction of Ca^{++}-induced *M. jannaschii* FtsZ sheets revealed that they are composed of antiparallel double protofilaments (Löwe and Amos, 1999). These FtsZ protofilaments, with a longitudinal spacing of approximately 43 Å, could be very well fitted with an atomic model of the FtsZ protofilament derived from the X-ray structure of FtsZ (Löwe and Amos, 1998) and the tubulin protofilament (Nogales *et al.*, 1998b). If only GTP is added, FtsZ assembles mostly into a network of straight filaments that are not well aligned and the filament bundles vary in thickness (Bramhill and Thompson, 1994; Mukherjee and Lutkenhaus, 1994; Erickson, 1995). None of these three classes of FtsZ polymers is well suited for the task FtsZ faces inside the cell. It has been estimated that there are around 15 000 FtsZ molecules per *E. coli* cell (Dai and Lutkenhaus, 1992; Lu *et al*., 1998). If a continuous ring assembles around the septum

FtsZ must form a fairly uniform polymer. Single filaments appear to be too short and have a radius of curvature (Erickson and Stoffler, 1996; Erickson *et al.*, 1996) incompatible with the inner cell surface. Furthermore, if the bending of protofilaments would generate force (Lu *et al*., 2000), each subunit contact in the protofilament would have to sustain the overall force applied to the membrane, which seems unlikely. Sheets are not well suited because there is no natural boundary for growth in the lateral direction. Poorly aligned bundles of protofilaments lack the required order and tend to form a network that is incompatible with ring formation. During our efforts to obtain Ca^{++}-induced sheets of *M. jannaschii* FtsZ (Löwe and Amos, 1999), most of the polymers formed appeared to be helical tubes but precipitated into a tight mass. We obtained a few pictures of free helical tubes but were unable to produce more. Two recent studies (Trusca *et al*., 1998; Lu *et al*., 2000) reported similar tubes of *E. coli* FtsZ obtained with GTP or GDP and the addition of DEAE dextran, confirming earlier reports of the existence of helical FtsZ tubes (Bramhill and Thompson, 1994; Mukherjee and Lutkenhaus, 1994; Erickson, 1995). Here, we present conditions that yield large quantities of helical *M. jannaschii* FtsZ tubes using the GTP analogue GMPCPP [guanylyl-(α,β)-methylene-diphosphate]. These tubes are related to the Ca^{++}-induced tubes and sheets and present an attractive hypothesis for the structure of the *in vivo* FtsZ polymer.

Results

Purified FtsZ1 protein from *M. jannaschii* has been polymerised into helical tubes under three different conditions. Condition P1 (see Materials and Methods) is the condition that has been used to obtain Ca^{++}-induced sheets (Löwe and Amos, 1999). The protein 'precipitates' upon addition of calcium and sheets form in solution. The insoluble protein consists almost exclusively of 'cables', helical FtsZ tubes that are very hydrophobic and are difficult to observe under the electron microscope. The few acceptable pictures that we were able to obtain all produce a helical diffraction pattern. Conditions P2 and P3 use GMPCPP at

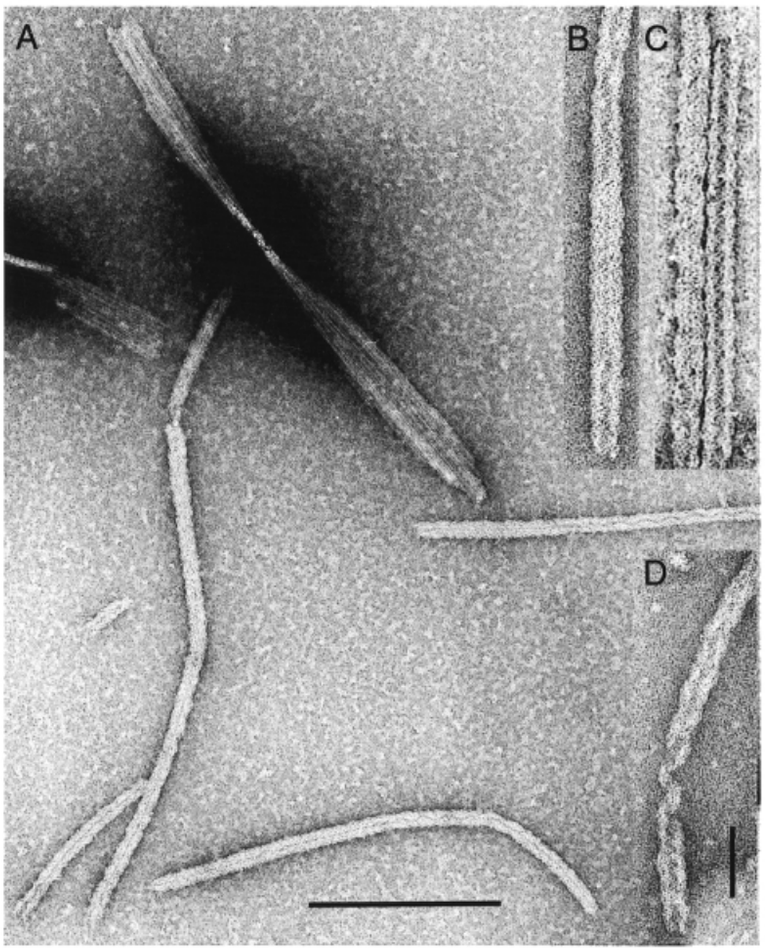

Fig. 1 FtsZ Polymers from *M. jannaschii* in the Presence of GMPCPP and Magnesium.
(A) Low magnification overview showing the presence of tubes and sheets on the same grid. Both forms of FtsZ polymer form with good yield and no apparent unspecific aggregation is visible. Scale bar: 500 nm. (B) Helical FtsZ tube whose center is more heavily stained at its two ends. (C) A filled and an empty helical FtsZ tube side by side in the same preparation, polymerisation condition P2 (see Materials and Methods). (D) A partially unwound helical tube (condition P3). Scale bar for (B) – (D): 100 nm.

10 mM and 2 mM, respectively. Both of these conditions produce sheets and cables with high yield as shown in Figure 1A. Condition P3 produced some tubes that show obvious unwinding, as shown in Figure 1D. The unwinding demonstrates the helical nature of the tubes as they are composed of curved ribbons of protofilaments. Many of the tubes assembled under condition P3 are empty (Figures 1C and 2C), whereas tubes assembled under condition P2 show stain exclusion everywhere, indicating that the core of the helix is filled with protein (Figure 1A, 2B). Some tubes were only partially empty, usually at either end (Figure 1B). Not many stretches of tubes were straight over long distances and most had to be straightened, as described under Materials and Methods, in order to obtain clear diffraction patterns. Representative tubes from the three polymerisation conditions and their diffraction patterns are shown in Figure 2. Tubes assembled in the presence of calcium show layer lines at repeats of 144 Å and 72 Å (Figure 2D) as published earlier (Löwe and Amos, 1999). Tubes assembled in the presence of GMPCPP show repeats of ~ 200 Å, 100 Å, 67 Å, and 50 Å (Figure 2E, F). The patterns from filled and empty GMPCPP tubes are similar, suggesting that the core filaments of the filled tubes either do not contribute to the diffraction patterns or that their symmetry is related to that of the outer shell. In the case of both Ca^{++}-induced and GMPCPP-induced tubes, all of the obvious layerlines are merely different orders of only one cell dimension of the helical surface lattice, that is, the spacing between groups of helical filaments. We have not yet identified any layerlines arising from a subunit periodicity along the filaments. We determined the number of separate filament groups from the two sets of diffraction patterns. The peaks on opposite sides of the Ca^{++}-tube 144 Å and the GMPCPP-tube 200 Å layerlines were clearly out of phase, indicating an odd-order helical family, and the positions of the first peaks were consistent with a

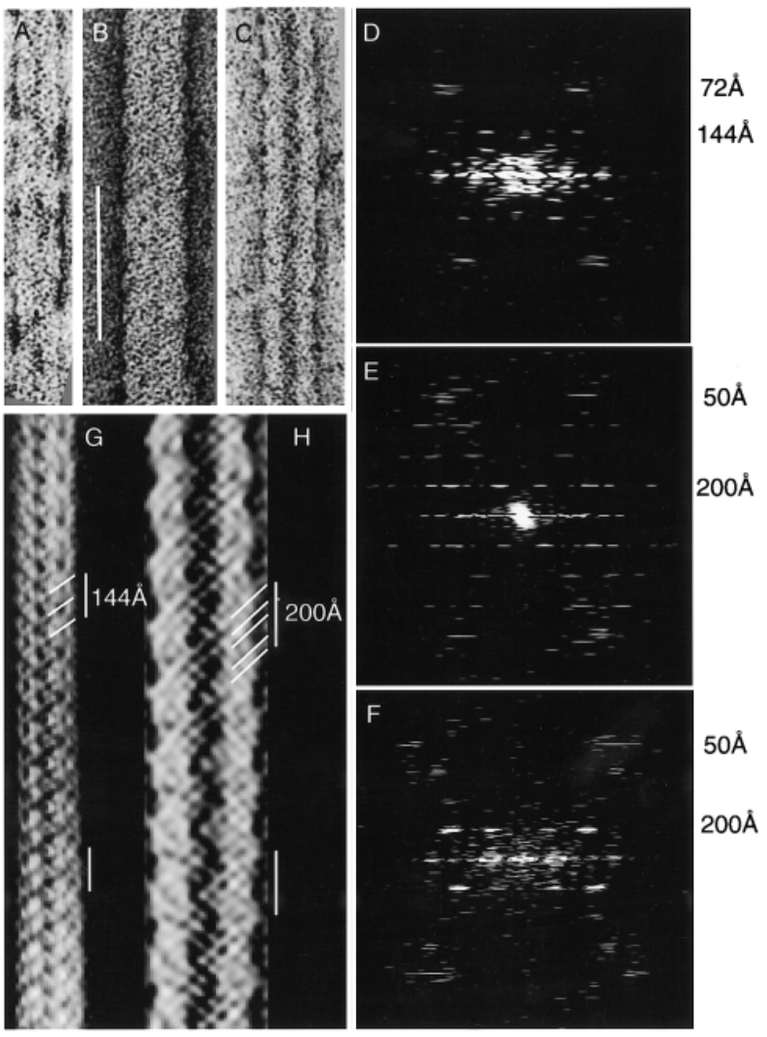

Fig. 2 Helical Tubes of FtsZ, Their Diffraction Patterns and Filtered Images.
(A, D) Ca^{++}-GTP helical FtsZ tube and its diffraction pattern (a different example from that previously published in Löwe and Amos, 1999). Scale bar: 100 nm. (B, E) Filled GMPCPP FtsZ tube and its diffraction pattern. (C, F) Empty GMPCPP tube and its diffraction pattern. (G, H) Filtered images from images (A) and (C). The repeat length is marked alongside. In (G), a repeat includes 2 filaments, 62 Å apart and running at an angle of 30°. In (H), four filaments at an angle of 44° make up the repeat. Their sideways separations appears to be ~ 37 Å, ~ 30 Å, ~ 43 Å and ~ 30 Å, but the upper two of the marked filaments are at a larger radius.

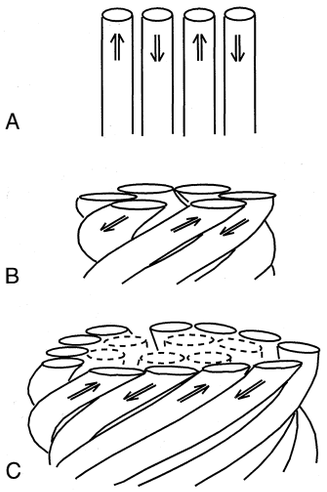

Fig. 3 Proposed Relationship between Sheets and Tubes.
(A) Sheets of *M. jannaschii* FtsZ were shown (Löwe and Amos, 1999) to consist of thick filaments (parallel pairs of protofilaments). Adjacent pairs of thick filaments are anti-parallel.
(B) Each Ca^{++}-GTP tube is made up of 6 helically-twisted thick filaments. Pairing of the thick filaments means that there is a family of three identical helical units.
(C) A GMPCPP tube consists of 3 independent groups of 4 filaments, each of which probably corresponds to a thick filament (see text). The filled tubes appear to contain additional filaments (dashed lines) but they are not sufficiently well-ordered in our specimens for their number and arrangement to be determined.

3-start family (Figure 3B). The phases and first-peak positions on the higher-order layerlines supported this assignment. Thus, the layerlines in the Ca^{++}-tube pattern can be indexed as (3,1) and (6,2); those in the GMPCPP patterns can be indexed as (3,1), (6,2), (9,3) and (12,4). We made filtered images by masking out everything in the diffraction patterns apart from the above-mentioned layerlines and reverse Fourier transforming. Examples are shown in Figure 2G and 2H. From such images it can be seen that a group of filaments producing the 144 Å longitudinal spacing of the Ca^{++}-induced tubes consists of a pair of filaments. Thus, the second layerline (6,2) can be directly related to a family of 6 ~ 62 Å wide filaments running in parallel around the helical axis, with a slope of ~ 30° and a pitch of ~ 430 Å (3 × 144 Å). In the case of the GMPCPP-induced tubes, groups producing the ~ 200 Å longitudinal spacing consist of 4 unequally-spaced filaments, with a slope of ~ 44° and a pitch of ~ 600 Å. Thus, the GMPCPP tubes have a total of 12 filaments running in parallel around the axis and the fourth layerline (12,4) corresponds to their average longitudinal spacing of 50 Å. Two of the 4 filaments tend to appear brighter than the others (see Figure 2H) and lead to bulgy outlines at the sides of the tube, suggesting that they run at slightly higher radii than the darker pair, which may be masked by negative stain lying in grooves between the ridges formed by the outer pair of filaments. The distance between the resolved filaments is small, as compared with the Ca^{++}-induced tubes. The spacing would be compatible with the broadest width of individual protofilaments. However, the empty tubes are too thick (~ 100 Å) to be made up of one layer of protofilaments. It therefore seems likely that the GMPCPP tubes also consist of thick filaments like those in the sheets and the Ca^{++}-GTP tubes. The distances between neighbouring filaments probably appear foreshortened because of their slightly different radial positions. Very low resolution 3D re-

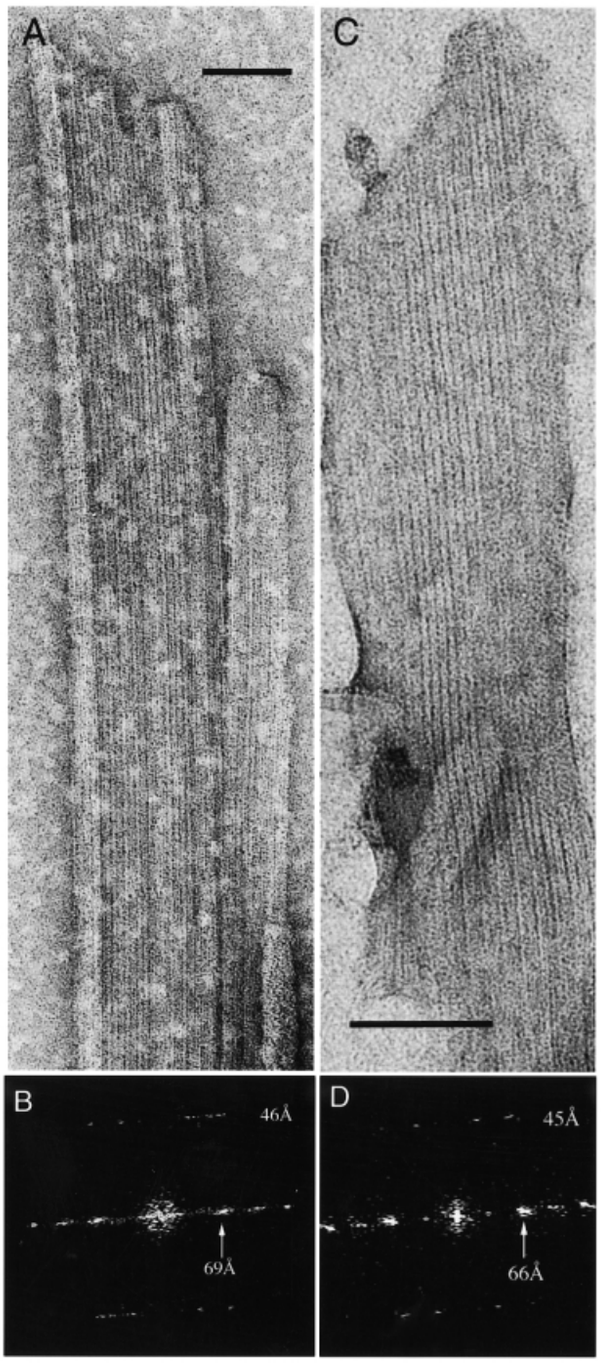

Fig. 4 Sheets of FtsZ from *M. jannaschii* Grown in the Presence of GMPCPP.
(A, C) FtsZ sheets assembled under condition P2. The left-hand edge of (A) consists of a roll of straight filaments. (B, D) Diffraction patterns from parts of (A) and (C). Spacings marked alongside the diffraction patterns are based on the nominal magnification. Scale bars: 100 nm.

constructions (sketched in Figure 3C) provided support for this interpretation of the filament arrangement.

Diffraction patterns from flat pieces of sheets assembled in the presence of GMPCPP (Figure 4) are closely similar to patterns obtained earlier from Ca^{++}-induced sheets (Löwe and Amos, 1999). These sheets also appear to consist of antiparallel pairs of thick filaments with a longitudinal subunit repeat of 43 – 46 Å and a filament separation of 65 – 70 Å. The only apparent difference is whereas Ca^{++}-induced sheets were often twisted in the form of taut ribbons, GMPCPP-induced sheets appeared less tense and sometimes became rolled up at their edges (Figure 4A) or compressed sideways.

Discussion

The finding that FtsZ, the bacterial tubulin homologue, forms a ring around the invaginating septum prompted the intuitive hypothesis that FtsZ forms a polymer during septation (Bi and Lutkenhaus, 1991; Lutkenhaus, 1993). Although no direct evidence for FtsZ involvement in force generation has been obtained so far, it is generally thought that force is generated either by motor proteins moving on FtsZ tracks or by FtsZ polymer dynamics analogous to microtubule or F-actin function. It is clear that FtsZ forms tubulin-like protofilaments (Erickson, 1995; Löwe and Amos, 1999) and that FtsZ plays a very direct role in the placement of additional components of the septum, as indicated by an insertion mutant that assembles spirals instead of rings (Bi and Lutkenhaus, 1992; Addinall and Lutkenhaus, 1996). Unfortunately, ultrastructural information about the septum and the *in vivo* FtsZ polymer has not been obtained so far. In the absence of knowledge about FtsZ's structure in the Z-ring we can only try to find *in vitro* conditions for FtsZ polymerisation that have the following characteristics: the polymerisation conditions should be universal and work for most FtsZ proteins with the same resulting polymer. The condition should yield an ordered polymer that does not form an irregular network. Furthermore, the functional polymer should be formed from only 10 – 20 protofilaments or less: the estimate of 15 000 FtsZ molecules per cell (Dai and Lutkenhaus, 1992; Lu *et al*., 1998) would translate into about 60 – 70 μm in length if all molecules assemble into protofilaments. For a septum of 1 μm diameter, this would give 10 – 20 protofilaments in the Z-ring, if FtsZ forms a continuous polymer. Each polymer would have fewer protofilaments if the Z-ring is made up of discontinuous and overlapping polymers, as in the eukaryotic cytokinetic actin structure which performs a similar, if not identical, function to the Z-ring in bacterial cell division. FtsZ has been polymerised *in vitro* to form curved thin filaments, sheets and protofilament bundles. None of these polymer forms seem to be suitable for FtsZ's role in the cell. When we investigated the Ca^{++}-induced formation of sheets of FtsZ we detected helical tubes but were not able to produce enough acceptable pictures for a detailed investigation. Two recent reports Trusca *et al*., 1998; Lu *et al*., 2000) presented similar helical tubes using FtsZ from *E. coli* and DEAE dextran/GDP. In our opinion, the helical FtsZ tubes represent the most likely hypothesis presented so far for the *in vivo* FtsZ polymer. Although we do not know which of the three forms of tube we have assembled is most likely to occur in a cell, each type consists of a defined and small number of protofilaments per length unit, is flexible enough to bend around the constricting septum and does not stick together to form a network of filaments. The last requirement mentioned above, a polymerisation condition that is universal or at least transferable from one protein to the other is not fulfilled, as *M. jannaschii* FtsZ does not form tubes under the conditions reported for *E. coli* FtsZ (Trusca *et al*., 1998; Lu *et al*., 2000; data not shown). This, however, may not be very surprising as *M. jannaschii* is a hyperthermophilic archaeon and grows above 80 °C. It is surprising to find that we can produce helical tubes with *M. jannaschii* FtsZ using the supposedly non-hydrolysable GTP analogue GMPCPP, as FtsZ is thought to form straight filaments when bound to GTP and curved protofilaments when bound to GDP (Lu and Erickson, 1997; Lu *et al*., 2000). Clearly, helical FtsZ tubes are made from curved filaments. When GMPCPP is replaced with GDP or GTP in our experiments, no polymer is formed or bundles of straight filaments form. One explanation for the formation of curved filaments in the presence of GMPCPP is slow hydrolysis, which we can observe when crystals of FtsZ are soaked with GMPCPP and left for prolonged periods of time (not shown). GMPCPP has been found to be hydrolysed by tubulin, although much more slowly than GTP (Hyman *et al*., 1992), but its hydrolysis by FtsZ has not yet been investigated. In solution, GMPCPP hydrolysis by FtsZ is expected to be much faster than in a crystal because of assembly-dependent GTPase activation. GTP may not induce helical tubes of *M. jannaschii* FtsZ because protofilament extension under our *in vitro* conditions may be too fast for the formation of ordered polymers. DEAE dextran, which could substitute for an accessory protein in aiding the assembly of *E. coli* FtsZ, seems not to have any influence on the *M. jannaschii* FtsZ polymerisation process (data not shown).

We have investigated helical tubes formed under two different conditions. Insoluble tubes formed in the presence of calcium while more soluble tubes formed reliably in the presence of GMPCPP. Analysis of diffraction patterns and filtered images of these tubes allowed us to determine their filament substructure. Both tubes are 3-start helices and differ mainly in the number of subfilaments. The calcium-induced tubes contain 2 subfilaments in a group, whereas the GMPCPP tubes contain 4 subfilaments, giving 6 and 12 subfilaments per tube. The spacing orthogonal to the subfilament direction, inclined by 30 – 45° from the tube axis, is ~ 60 Å for the calcium tubes. It is less for the unequally-spaced subfilaments of the GMPCPP tubes but their overall separation, including the radial differences, is probably similar. Since both types of helical FtsZ tubes have been obtained under conditions that form sheets as well, we compared the sheets obtained in the

presence of GMPCPP with the Ca^{++}-induced sheets (Löwe and Amos, 1999) and found them to have very similar lattice constants and diffraction patterns. We therefore conclude that the GMPCPP sheets contain alternating antiparallel thick filaments, each composed of two parallel FtsZ protofilaments, like the Ca^{++}-induced sheets. A spacing of 50 – 60 Å in the tubes, which has been seen in the *E. coli* helical FtsZ tubes as well (Lu *et al*., 2000), could be generated by a double protofilament or a single protofilament. In an atomic model of the FtsZ protofilament, the thinnest diameter is 25 Å and the thickest 50 Å, excluding helix H0 (Löwe and Amos, 1998, 1999). We tend to think that the *M. jannaschii* FtsZ tubes are composed of double protofilaments as well, since they form under the same conditions as the sheets (see Figure 1), and that the tube and sheet polymer forms may represent the parallel and antiparallel subfilament arrangement. The nature of the subfilaments could be investigated using cryo-EM and higher resolution three-dimensional image reconstruction.

Polymerisation condition P2 yielded filled tubes, whereas condition P3 yielded empty or partially filled tubes. We were not able to determine what the core consists of but it may be another protein structure following the helical symmetry.

The helical FtsZ tubes found in this study and by others are very different from normal eukaryotic microtubules. Microtubules contain straight or almost straight protofilaments formed with β-tubulin in the GTP state, depending of the number of protofilaments (Wade *et al*., 1990). After hydrolysis of GTP to GDP, the relaxed protofilament would prefer to adopt a curved conformation, thus giving dynamic instability to the microtubule (Desai and Mitchison, 1997). This mechanism stores energy in the microtubule lattice during tube formation so that an additional source of energy is not essential for disassembly (Mitchison and Kirschner, 1984). Since FtsZ tubes appear to contain significantly curved filaments, this polymer may not be dynamic and external factors may be required to disassemble the tubes. Here the role of GTP hydrolysis could be that of a lock, making disassembly unlikely. We think it is possible that GTP hydrolysis actually promotes lateral interactions between FtsZ protofilaments. FtsZ lacks the M-loop of tubulin (Nogales *et al*., 1999) that is responsible for the most important lateral interaction between tubulin protofilaments, so lateral interactions between FtsZ protofilaments may well be quite different from those in microtubules. Mitchison and Kirschner (1984) suggested that dynamic instability of microtubules was important in ensuring that microtubules assembled without proper initiation would automatically soon disassemble. The dynamic property of FtsZ protofilaments is likely to serve a similar purpose. As mentioned above, it seems to be necessary for practically all of the molecules present in the cell to assemble in a specific region. The average concentration of FtsZ throughout the cell may be insufficient for unassisted assembly into tubes although it is probably above the critical concentration of 20 to 50 μg/ml for polymerisation into smaller structures (Lu et al., 1998; Mukherjee and Lutkenhaus, 1998; Mukherjee and Lutkenhaus, 1999). Thus, it should only be necessary for individual protofilaments and small bundles to be dynamically unstable.

Microtubules are the tracks of motor proteins that move along protofilaments to produce linear force (Hirokawa, 1998). A helical tube does not seem to be optimal for this task due to topological implications, although it could rotate if neither end is fixed and the motors are involved in holding it on to the membrane.

To observe the subunit repeat along the protofilaments it will be necessary to use cryo-EM to obtain higher resolution images and to obtain less bent polymers. Three-dimensional reconstruction of ice-embedded helical FtsZ polymers will also allow for investigation of FtsZ:protein complexes with components of the septum interacting with FtsZ like FtsA, ZipA, FtsQ, and others. The helical tubes may also be very useful for setting up motility assays under the DIC light microscope with FtsZ filaments and bacterial lysates or purified proteins, to search for bacterial motor proteins. Prelimary experiments indicate that they are large enough to be visible by light microscopy.

The helical FtsZ cables presented in this study form with high yield. In addition to their potential as important tools for the investigation of FtsZ:protein complexes with cryo-EM and video-enhanced light microscopy, they provide a promising hypothesis for the *in vivo* polymer of FtsZ.

Materials and Methods

FtsZ1 from *Methanococcus jannaschii* was expressed and purified as described before (Löwe, 1998). The protein was stored at 4 °C in 20 mM TRIS, 1 mM EDTA, 1 mM Na-azide. Nucleotides were used as neutralised 100 mM stock solutions (pH 7.0). GMPCPP was synthesised as described by Hyman *et al.* (1992). For FtsZ tube formation, three different polymerisation conditions were used: P1 (as previously published in Löwe and Amos, 1999): 8 mM magnesium acetate, 8 mM calcium chloride and 8 mM GTP were added to FtsZ1 to give a final protein concentration of 2 mg/ml. The cloudy reaction product was vortexed for 10 s. Polymerisation condition P2: 10 mM GMPCPP and 20 mM magnesium acetate were mixed with FtsZ1 to give a final protein concentration of 0.8 mg/ml. P2 yields sheets and filled tubes. P3: as P2 but with 2 mM GMPCPP and 4 mM magnesium acetate. P3 yields exclusively empty tubes. All reactions were incubated for 20 min at 37 °C. Samples were negatively stained with 1% uranyl acetate and observed in a Philips 208 80 kV electron microscope. Electron micrographs used for image processing were photographed at magnifications between 25 000 and 63 000. They were scanned with a Zeiss SCAI scanner at 28 or 14 micrometer step size and processed using the MRC package of programs (Crowther *et al*., 1996). After spline-fitting a line down the axis of each image of a curved polymer, unbending was achieved by bilinear interpolation (Egelman, 1986). The straightened image was boxed and floated and its Fourier transform (512 × 1024 or 512 × 512, depending on the length of polymer available) was calculated. Filtered images were obtained by masking out unwanted regions of the Fourier transform and calculating a reverse Fourier transformation. For a more detailed analysis, complex data along each layerline were extracted and the phases on opposite sides

of the meridian were compared. For each possible indexing scheme, a search was made over a range of x-shifts and tilt angles (out of the plane normal to the direction of view) to find values that would give an overall minimum for the amplitude-weighted phase differences (or differences-π, in the case of odd-order helical families) at equal distances from the meridian. The values of the overall minima provided an indication of the most likely indexing scheme. After appropriate correction of the phases, each Fourier transform yielded 2 datasets, from the 'near' and 'far' sides of the image. The phases in each dataset were then compared to estimate the z-shift and rotation around the helix axis required to bring each particle into conjunction with a chosen reference. The shifts that minimised the weighted difference in the phases were found by searching values that covered a complete repeat. Agreement between the near and far sides of a particular image was used as an indication of the quality of the data. The phases in each dataset were corrected to shift the structure into the reference orientation and an average of the datasets was used to reconstruct 3D images for comparison with the recorded electron micrographs and filtered images.

Acknowledgements

This work was carried out with some support from the Human Frontier Science Program. We thank Dr. T. J. Mitchison (Harvard Medical School) for advice about GMPCPP and are grateful to Dr. N. Caplan and Professor G. M. Blackburn (Department of Chemistry, University of Sheffield) who synthesised this nucleotide for us.

References

Addinall, S.G., and Lutkenhaus, J. (1996). FtsZ-spirals and -arcs determine the shape of the invaginating septa in some mutants of *Escherichia coli*. Mol. Microbiol. *22*, 231 – 237.

Bi, E., and Lutkenhaus, J. (1991). Ftsz ring structure associated with division in *Escherichia coli*. Nature *354*, 161 – 164.

Bi, E., and Lutkenhaus, J. (1992). Isolation and characterization of FtsZ alleles that affect septal morphology. J. Bacteriol. *174*, 5414 – 5423.

Bramhill, D. (1997). Bacterial cell division. Annu. Rev. Cell Dev. Biol. *13*, 395 – 424.

Bramhill, D., and Thompson, C.M. (1994). GTP-dependent polymerization of *Escherichia coli* FtsZ protein to form tubules. Proc. Natl. Acad. Sci. USA *91*, 5813 – 5817.

Crowther, R.A., Henderson, R., and Smith, J. M. (1996). MRC image processing programs. J. Struct. Biol. *116*, 9 – 16.

Dai, K., and Lutkenhaus, J. (1992). The proper ratio of FtsZ to FtsA is required for cell division to occur in *Escherichia coli*. J. Bacteriol. *174*, 6145 – 6151.

Desai, A., and Mitchison, T.J. (1997). Microtubule polymerization dynamics. Annu. Rev. Cell Dev. Biol. *13*, 83 – 117.

Donachie, W.D. (1993). The cell-cycle of *Escherichia coli*. Annu. Rev. Microbiol. *47*, 199 – 230.

Egelman, E.H. (1986). An algorithm for straightening images of curved filamentous structures. Ultramicroscopy *19*, 367 – 373.

Erickson, H.P. (1995). FtsZ, a prokaryotic homolog of tubulin? Cell *80*, 367 – 370.

Erickson, H. P. (1998). Atomic structures of tubulin and FtsZ. Trends Cell Biol. *8*, 133–137.

Erickson, H.P., and Stoffler, D. (1996). Protofilaments and rings, 2 conformations of the tubulin family conserved from bacterial Ftsz to alpha/beta and gamma-tubulin. J. Cell Biol. *135*, 5 – 8.

Erickson, H.P., Taylor, D.W., Taylor, K.A., and Bramhill, D. (1996). Bacterial cell division protein FtsZ assembles into protofilament sheets and minirings, structural homologs of tubulin polymers. Proc. Natl. Acad. Sci. USA *93*, 519 – 523.

Hirokawa, N. (1998). Kinesin and dynein superfamily proteins and the mechanism of organelle transport. Science *279*, 519 – 526.

Hyman, A.A., Salser, S., Drechsel, D.N., Unwin, N., and Mitchison, T.J. (1992). Role of GTP hydrolysis in microtubule dynamics: information from a slowly hydrolyzable analogue, GMPCPP. Mol Biol Cell *3*, 1155 – 1167.

Löwe, J. (1998). Crystal structure determination of FtsZ from *Methanococcus jannaschii*. J. Struct. Biol. *124*, 235 – 243.

Löwe, J., and Amos, L.A. (1998). Crystal structure of the bacterial cell-division protein FtsZ. Nature *391*, 203 – 206.

Löwe, J., and Amos, L.A. (1999). Tubulin-like protofilaments in Ca^{2+}-induced FtsZ sheets. EMBO J. *18*, 2364 – 2371.

Lu, C.L., and Erickson, H.P. (1999). The straight and curved conformation of FtsZ protofilaments – evidence for rapid exchange of GTP into the curved protofilament. Cell Struct. Funct. *24*, 285 – 290.

Lu, C.L., Stricker, J., and Erickson, H.P. (1998). FtsZ from *Escherichia coli*, *Azotobacter vinelandii*, and *Thermotoga maritima* - quantitation, GTP hydrolysis, and assembly. Cell Mot. Cytoskel. *40*, 71 – 86.

Lu, C.L., Reedy, M., and Erickson, H.P. (2000). Straight and curved conformations of FtsZ are regulated by GTP hydrolysis. J. Bacteriol. *182*, 164 – 170.

Lutkenhaus, J. (1993). FtsZ ring in bacterial cytokinesis. Mol. Microbiol. *9*, 403 – 409.

Lutkenhaus, J., and Addinall, S.G. (1997). Bacterial cell division and the Z ring. Annu. Rev. Biochem *66*, 93 – 116.

Mitchison, T.J., and Kirschner, M. W. (1984). Dynamic instability of microtubule growth. Nature *312*, 237 – 242.

Mukherjee, A., and Lutkenhaus, J. (1994). Guanine nucleotide-dependent assembly of FtsZ into filaments. J. Bacteriol. *176*, 2754 – 2758.

Mukherjee, A., and Lutkenhaus, J. (1998). Dynamic assembly of FtsZ regulated by GTP hydrolysis. EMBO J. *17*, 462 – 469.

Mukherjee, A., and Lutkenhaus, J. (1999). Analysis of FtsZ assembly by light scattering and determination of the role of divalent metal cations. J. Bacteriol. *181*, 823 – 832.

Nogales, E., Downing, K.H., Amos, L.A., and Löwe, J. (1998a). Tubulin and FtsZ form a distinct family of GTPases. Nature Struct. Biol. *5*, 451 – 458.

Nogales, E., Wolf, S.G., and Downing, K.H. (1998b). Structure of the α/β-tubulin dimer by electron crystallography. Nature *391*, 199 – 203.

Nogales, E., Whittaker, M., Milligan, R.A., and Downing, K.H. (1999). High-resolution model of the microtubule. Cell *96*, 79 – 88.

Rothfield, L., Justice, S., and GarciaLara, J. (1999). Bacterial cell division. Annu. Rev. Gen. *33*, 423 – 448.

Trusca, D., Scott, S., Thompson, C., and Bramhill, D. (1998). Bacterial SOS checkpoint protein SulA inhibits polymerization of purified FtsZ cell division protein. J. Bacteriol. *180*, 3946 – 3953.

Wade, R.H., Chrétien, D., and Job, D. (1990). Characterization of microtubule protofilament numbers. How does the surface lattice accommodate? J. Mol. Biol. *212*, 775 – 786.

Yu, X.C., and Margolin, W. (1997). Ca^{2+}-mediated GTP-dependent dynamic assembly of bacterial cell division protein FtsZ into asters and polymer networks *in vitro*. EMBO J. *16*, 5455 – 5463.

Received May 24, 2000; accepted July 14, 2000